

# Pseudoscalar and vector mesons as $q\bar{q}$ bound states

A. Krassnigg<sup>1</sup> and P. Maris<sup>2</sup>

<sup>1</sup> Physics Division, Argonne National Laboratory, Argonne, IL 60439

<sup>2</sup> Department of Physics and Astronomy, University of Pittsburgh, Pittsburgh, PA 15260

E-mail: andreas.krassnigg@anl.gov, pim6@pitt.edu

**Abstract.** Two-body bound states such as mesons are described by solutions of the Bethe–Salpeter equation. We discuss recent results for the pseudoscalar and vector meson masses and leptonic decay constants, ranging from pions up to  $c\bar{c}$  bound states. Our results are in good agreement with data. Essential in these calculation is a momentum-dependent quark mass function, which evolves from a constituent-quark mass in the infrared region to a current-quark mass in the perturbative region. In addition to the mass spectrum, we review the electromagnetic form factors of the light mesons. Electromagnetic current conservation is manifest and the influence of intermediate vector mesons is incorporated self-consistently. The results for the pion form factor are in excellent agreement with experiment.

## 1. Dyson–Schwinger equations

The set of Dyson–Schwinger equations form a Poincaré covariant framework within which to study hadrons [1, 2]. In rainbow-ladder truncation, they have been successfully applied to calculate a range of properties of the light pseudoscalar and vector mesons, see Ref. [2] and references therein.

The DSE for the renormalized quark propagator  $S(p)$  in Euclidean space is [1]

$$S(p)^{-1} = i Z_2(\zeta) \not{p} + Z_4(\zeta) m(\zeta) + Z_1(\zeta) \int \frac{d^4 q}{(2\pi)^4} g^2 D_{\mu\nu}(p-q) \frac{\lambda^i}{2} \gamma_\mu S(q) \Gamma_\nu^i(q, p), \quad (1)$$

where  $D_{\mu\nu}(p-q)$  and  $\Gamma_\nu^i(q; p)$  are the renormalized dressed gluon propagator and quark-gluon vertex, respectively. The most general solution of Eq. (1) has the form  $S(p)^{-1} = i \not{p} A(p^2) + B(p^2)$ , renormalized at spacelike  $\zeta^2$  according to  $A(\zeta^2) = 1$  and  $B(\zeta^2) = m(\zeta)$  with  $m(\zeta)$  the current quark mass.

Mesons are described by solutions of the homogeneous Bethe–Salpeter equation (BSE)

$$\Gamma_H(p_+, p_-; P) = \int \frac{d^4 q}{(2\pi)^4} K(p, q; P) S(q_+) \Gamma_H(q_+, q_-; P) S(q_-), \quad (2)$$

at discrete values of  $P^2 = -M_H^2$ , where  $M_H$  is the meson mass. In this equation,  $p_+ = p + P/2$  and  $p_- = p - P/2$  are the outgoing and incoming quark momenta respectively, and similarly for  $q_\pm$ . The kernel  $K$  is the renormalized, amputated  $q\bar{q}$  scattering kernel that is irreducible with respect to a pair of  $q\bar{q}$  lines. Together with the canonical normalization condition for  $q\bar{q}$  bound states, Eq. (2) completely determines the bound state Bethe–Salpeter amplitude (BSA)  $\Gamma_H$ .

Different types of mesons, such as pseudoscalar or vector mesons, are characterized by different Dirac structures.

To solve the BSE, we use the ladder truncation,

$$K(p, q; P) \rightarrow -4\pi\alpha^{\text{eff}}((p - q)^2) D_{\mu\nu}^0(p - q) \frac{\lambda^i}{2} \gamma_\mu \otimes \frac{\lambda^i}{2} \gamma_\nu, \quad (3)$$

in conjunction with the rainbow truncation for the quark DSE, Eq. (1):  $\Gamma_\nu^i(q, p) \rightarrow \frac{\lambda^i}{2} \gamma_\nu$  and  $Z_1 g^2 D_{\mu\nu}(k) \rightarrow 4\pi\alpha^{\text{eff}}(k^2) D_{\mu\nu}^0(k)$ , with  $k = p - q$ . Here,  $D_{\mu\nu}^0(k)$  is the free gluon propagator in Landau gauge, and  $\alpha^{\text{eff}}(k^2)$  an effective quark-quark interaction, which reduces to the one-loop running coupling of perturbative QCD (pQCD) in the perturbative region. This truncation preserves both the vector Ward–Takahashi identity (WTI) for the  $q\bar{q}\gamma$  vertex and the axial-vector WTI, independent of the details of the effective interaction. The latter ensures the existence of massless pseudoscalar mesons associated with dynamical chiral symmetry breaking (D $\chi$ SB) in the chiral limit [3, 4]. In combination with an impulse approximation, the former ensures electromagnetic current conservation [5, 6].

## 2. Quark propagator: an overview

A momentum-dependent quark mass function  $M(p^2) = B(p^2)/A(p^2)$  is central to QCD. In the perturbative region this mass function gives the one-loop perturbative running quark mass

$$M(p^2) \simeq \frac{\hat{m}}{\left(\frac{1}{2} \ln \left[p^2/\Lambda_{\text{QCD}}^2\right]\right)^{\gamma_m}}, \quad (4)$$

with the anomalous mass dimension  $\gamma_m = 12/(33 - 2N_f)$ . Dynamical chiral symmetry breaking means that this mass function is nonzero even though the current-quark masses are zero. In the chiral limit the mass function is [7]

$$M_{\text{chiral}}(p^2) \simeq \frac{2\pi^2\gamma_m}{3} \frac{-\langle\bar{q}q\rangle^0}{p^2 \left(\frac{1}{2} \ln \left[p^2/\Lambda_{\text{QCD}}^2\right]\right)^{1-\gamma_m}}, \quad (5)$$

with  $\langle\bar{q}q\rangle^0$  the renormalization-point-independent vacuum quark condensate [3].

It is a longstanding prediction of DSE studies in QCD that the dressed quark propagator receives strong momentum-dependent corrections at infrared momenta, see e.g. Refs. [1, 2] and references therein. Provided that the (effective) quark-quark interaction reduces to the perturbative running coupling in the ultraviolet region, it is also straightforward to reproduce the asymptotic behavior of Eqs. (4) and (5) [8, 9]. Both these phenomena are illustrated in the left panel of Fig. 1. In this figure one can also see that the dynamical mass function of the  $u$  and  $d$  quarks becomes very similar to that of quarks in the chiral limit in the infrared region. This is a direct consequence of D $\chi$ SB, and leads to a mass function of the order of several hundred MeV for the light quarks in the infrared, providing one with a constituent mass for quarks inside hadrons, even though the corresponding current quark masses are only a few MeV.

These predictions were recently confirmed in lattice simulations of QCD [10–12]. Quantitative agreement between the lattice simulations and the DSE results for the quark propagator functions can be obtained within the rainbow truncation via a suitable choice for the effective quark-quark interaction [13]. Pointwise agreement for a range of quark masses requires this interaction to be flavor-dependent [14], suggesting that dressing the quark-gluon vertex  $\Gamma_\nu^i(q, p)$  is important. Indeed, both lattice simulations [15] and DSE studies [16–18] of this vertex indicate that  $\Gamma_\nu^i(q, p)$  deviates significantly from a bare vertex in the nonperturbative region. A (flavor-dependent) nonperturbative vertex dressing could make a significant difference for the solution of the quark DSE [16, 19], as can be seen from the right panel of Fig. 1. The consequences of a dressed vertex for the meson BSEs are currently being explored [16] and indications are that in the pseudoscalar and vector channels, the effects are small [16, 20, 21].

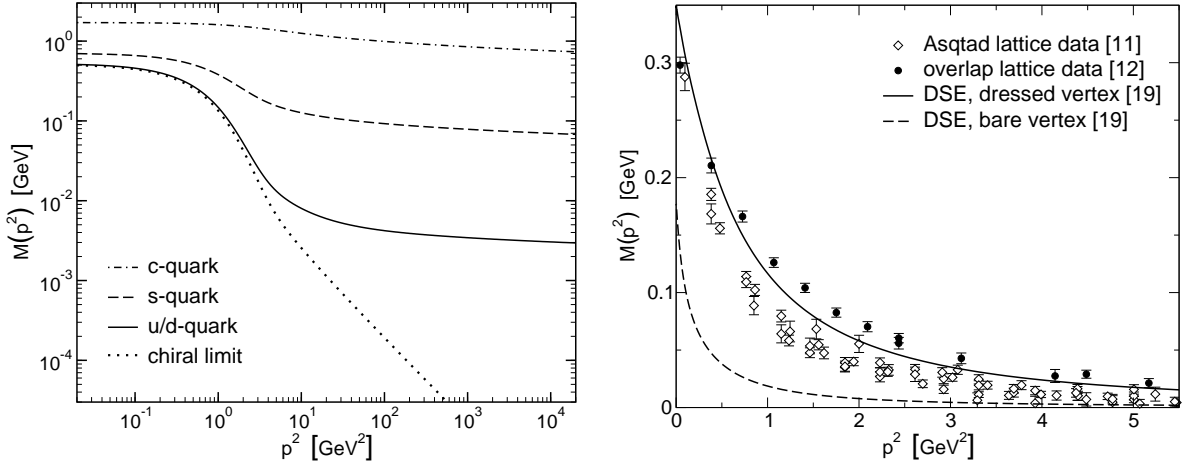


**Figure 1.** The dynamical quark mass function  $M(p^2)$  for different quark flavors (left, adapted from Ref. [3]) and a comparison of the chiral-limit quark mass function with the lattice data [11,12] (right, adapted from Ref. [19]).

### 3. Pseudoscalar mesons: ground and excited states

The meson spectrum contains three pseudoscalars with quantum numbers  $I^G(J^P)L = 1^-(0^-)S$  and masses below 2 GeV:  $\pi(140)$ ;  $\pi(1300)$ ; and  $\pi(1800)$ . In a constituent-quark model, these mesons are viewed as the first three members of a  $q\bar{q} n^1S_0$  trajectory, where  $n$  is the principal quantum number with the ground state  $\pi_0$  (the  $\pi(140)$ ), and the others are its first two radial excitations,  $\pi_1$  and  $\pi_2$ . The pseudoscalar trajectory is particularly interesting, because its lowest mass member is QCD's Goldstone mode. Therefore an explanation should describe both chiral symmetry and its dynamical breaking as well as a correlation of the ground and excited states via an approximately linear radial Regge trajectory. The latter is easily realized in Poincaré invariant quantum mechanics [22] but the former is not.

#### 3.1. Chiral symmetry

The chiral properties of QCD are manifest in the axial-vector WTI, which reads

$$P_\mu \Gamma_{5\mu}(q_+, q_-; P) = S^{-1}(q_+) i\gamma_5 + i\gamma_5 S^{-1}(q_-) - 2i m_q(\zeta) \Gamma_5(q_+, q_-; P), \quad (6)$$

with  $\Gamma_{5\mu}(q_+, q_-; P)$  and  $\Gamma_5(q_+, q_-; P)$  the renormalized dressed axial-vector and pseudoscalar vertices, each satisfying an inhomogeneous extension of Eq. (2). Equation (6) is an exact statement in QCD implying that the kernels of the quark DSE, Eq. (1), and of the BSEs have to be intimately related. A weak coupling expansion of the DSEs yields perturbation theory and satisfies this constraint, but is not useful in the study of intrinsically nonperturbative phenomena. However, a systematic and symmetry preserving nonperturbative truncation scheme exists [16, 20, 21], allowing for both elucidation and illustration of the consequences of the axial-vector WTI.

Pseudoscalar mesons appear as pole contributions to the axial-vector and pseudoscalar vertices at  $P^2 = -M_{\pi_n}^2$ . The residues of these poles are

$$f_{\pi_n} P_\mu = Z_2(\zeta) \int \frac{d^4 q}{(2\pi)^4} \text{Tr} [\gamma_5 \gamma_\mu S(q_+) \Gamma_{\pi_n}(q_+, q_-; P) S(q_-)], \quad (7)$$

$$i\rho_{\pi_n}(\zeta) = Z_4(\zeta) \int \frac{d^4 q}{(2\pi)^4} \text{Tr} [\gamma_5 S(q_+) \Gamma_{\pi_n}(q_+, q_-; P) S(q_-)], \quad (8)$$

both of which are gauge invariant and cutoff independent. It follows from Eq. (6) that these residues satisfy the following exact identity in QCD [4, 23]

$$f_{\pi_n} M_{\pi_n}^2 = 2m(\zeta) \rho_{\pi_n}(\zeta), \quad (9)$$

valid for every  $0^-$  meson [24], irrespective of the magnitude of the current quark mass [25].

For the  $\pi_0$ , D $\chi$ SB yields:  $\lim_{\hat{m} \rightarrow 0} f_{\pi_0} \neq 0$  and  $\lim_{\hat{m} \rightarrow 0} \rho(\zeta) = -2\langle \bar{q}q \rangle_\zeta^0 / f_{\pi_0}^0 \neq 0$ . Hence, the Gell-Mann–Oakes–Renner relation emerges as a corollary of Eq. (9) and the ground state pion is QCD’s Goldstone mode [4]. For the  $n \geq 1$  pseudoscalar mesons one has  $M_{\pi_{n \geq 1}} > M_{\pi_0}$  by assumption, and hence  $M_{\pi_{n > 0}} \neq 0$  in the chiral limit. Furthermore, the ultraviolet behavior of the quark-antiquark scattering kernel in QCD guarantees that  $\rho_{\pi_n}(\zeta)$  is finite in the chiral limit. Hence, it is a necessary consequence of chiral symmetry and the axial-vector WTI that  $f_{\pi_n}$  vanishes in the chiral limit for all excited pseudoscalar mesons (i. e. for all  $n > 0$ ) [24].

### 3.2. Numerical results

We now illustrate the exact results reviewed above in a model that both preserves QCD’s ultraviolet properties and exhibits D $\chi$ SB, namely the rainbow-ladder truncation of the set of DSEs. For the infrared behavior of the effective quark-quark interaction,  $\alpha^{\text{eff}}(k^2)$ , we employ an Ansatz [3, 26] that is sufficiently enhanced in the infrared to produce a realistic value for the vacuum quark condensate of about  $(240 \text{ GeV})^3$ . The model parameters, along with the quark masses [26, 27], are fitted to give a good description of the chiral condensate,  $M_{\pi/K/\eta_c}$  and  $f_\pi$ . The obtained quark propagator functions agree qualitatively with lattice simulations.

The main results for the pseudoscalar and vector meson masses and leptonic decay constants are summarized in Table 1 and illustrated in Fig. 2. Regarding the table one should note that the rainbow-ladder truncation gives “ideal” flavor mixing and the study uses  $\hat{m}_u = \hat{m}_d \neq \hat{m}_s \neq \hat{m}_c$ . Thus the first row simultaneously describes four degenerate mesons for each column, namely, a  $\{u\bar{d}, u\bar{u} - d\bar{d}, d\bar{u}\}$  isotriplet and a  $u\bar{u} + d\bar{d}$  isosinglet. The second row describes  $s\bar{s}$  mesons, and the third row  $c\bar{c}$  mesons. For vector mesons ideal mixing is a very good approximation, though this is not the case for the pseudoscalar ground states. However, the experimental degeneracy of the  $\pi(1300)$  and  $\eta(1295)$  suggests [28] that ideal mixing is almost realized for the excited pseudoscalar mesons. This supports the interpretation of the  $\eta(1295)$  and  $\eta(1470)$  as the radial excitations of the  $\eta(548)$  and  $\eta'(958)$ , with quark content almost entirely  $u\bar{u} + d\bar{d}$  and  $s\bar{s}$  respectively [27]. Figure 2 shows bound-state masses and leptonic decay constants for the ground and excited states of pseudoscalar mesons as well as ground-state vector-meson masses as functions of the current-quark mass. It illustrates that  $m_{\pi_0}$  vanishes in the chiral limit, while  $m_\rho$  and  $m_{\pi_1}$  do not; on the other hand,  $f_{\pi_1}$  vanishes in the chiral limit, while  $f_{\pi_0}$  does not.

**Table 1.** Results for the  $q\bar{q}$   $0^-$  ground and first radially excited states as well as  $q\bar{q}$   $1^-$  ground states. The current-quark masses are  $m_{u/d} = 5.4 \text{ MeV}$ ,  $m_s = 124 \text{ MeV}$ , and  $m_c = 1.34 \text{ GeV}$  at  $\zeta = 1 \text{ GeV}$ , and all quantities are given in GeV; for the leptonic decay constants we follow the conventions of Ref. [25, 26]. Experimental data are taken from [28] except for  $f_{\eta_c}$  [29].

$q$	$M_{\pi_0}$	$M_{\text{expt}}$	$f_{\pi_0}$	$f_{\text{expt}}$	$M_{\pi_1}$	$M_{\text{expt}}$	$f_{\pi_1}$	$M_V$	$M_{\text{expt}}$	$f_V$	$f_{\text{expt}}$
$u, d$	0.14	0.14	0.131	0.131	1.10	1.3	-0.002	0.74	0.77	0.206	0.22
$s$	0.70	—	0.182	—	1.41	1.47	-0.033	1.08	1.02	0.257	0.23
$c$	2.98	2.98	0.33	0.34	3.45	3.65	-0.15	3.13	3.10	0.33	0.41

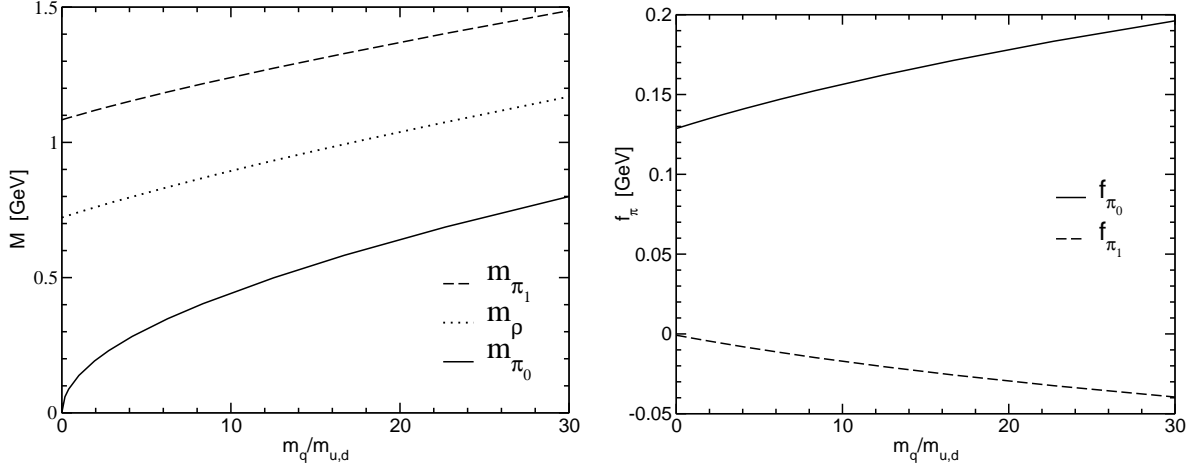


**Figure 2.** The masses  $M$  of the pseudoscalar ground and first radially excited states (left) and the corresponding weak decay constants (right) as functions of the current-quark mass  $m_q$ . For comparison, we also include the mass of the ground-state vector mesons.

Satisfaction of the axial-vector WTI can be checked by virtue of Eq. (9) for any pseudoscalar meson in Table 1. For the ground and excited states the inaccuracies are below 1% and 5%, respectively. The latter are larger because of: (1) the need to project out the ground state in order to calculate the excited state, (2) the smallness of  $f_{\pi_1}$  close to the chiral limit, and (3) the larger bound-state mass, leading to a larger region of analytic continuation for the quark DSE solution in the complex  $p^2$  plane.

#### 4. Electromagnetic form factors

Meson-meson-photon interactions can be described in generalized impulse approximation by

$$I^{abc}(P, Q, K) = \int \frac{d^4 q}{(2\pi)^4} \text{Tr}[S^a(q) \Gamma^{ab}(q, q'; P) S^b(q') \Gamma^{b\bar{c}}(q', q''; Q) S^c(q'') \Gamma^{c\bar{a}}(q'', q; K)], \quad (10)$$

where  $q - q' = P$ ,  $q' - q'' = Q$ ,  $q'' - q = K$ , and momentum conservation dictates  $P + Q + K = 0$ . In Eq. (10),  $S^i$  is the dressed quark propagator with flavor index  $i$ , and  $\Gamma^{i\bar{j}}(k, k'; P)$  stands for a generic vertex function with incoming quark flavor  $j$  and momentum  $k'$ , and outgoing quark flavor  $i$  and momentum  $k$ . Depending on the specific process under consideration, this vertex function could be a meson BSA or a quark-photon vertex.

The quark-photon vertex,  $\Gamma_{\mu}(p_+, p_-; Q)$ , with  $Q$  the photon momentum and  $p_{\pm}$  the quark momenta, is the solution of the inhomogeneous BSE

$$\Gamma_{\mu}(p_+, p_-; Q) = Z_2(\zeta) \gamma_{\mu} + \int \frac{d^4 q}{(2\pi)^4} K(p, q; Q) S(q_+) \Gamma_{\mu}(q_+, q_-; Q) S(q_-). \quad (11)$$

Solutions of the homogeneous version of Eq. (11) define vector meson bound states at timelike photon momenta  $Q^2 = -M_V^2$ . It follows that  $\Gamma_{\mu}(p_+, p_-; Q)$  has poles at these locations [6] (see also the vector-meson masses in Table 1).

##### 4.1. Pion and kaon elastic form factors

There are two diagrams that contribute to meson electromagnetic form factors: one with the photon coupled to the quark and one with the photon coupled to the antiquark respectively.

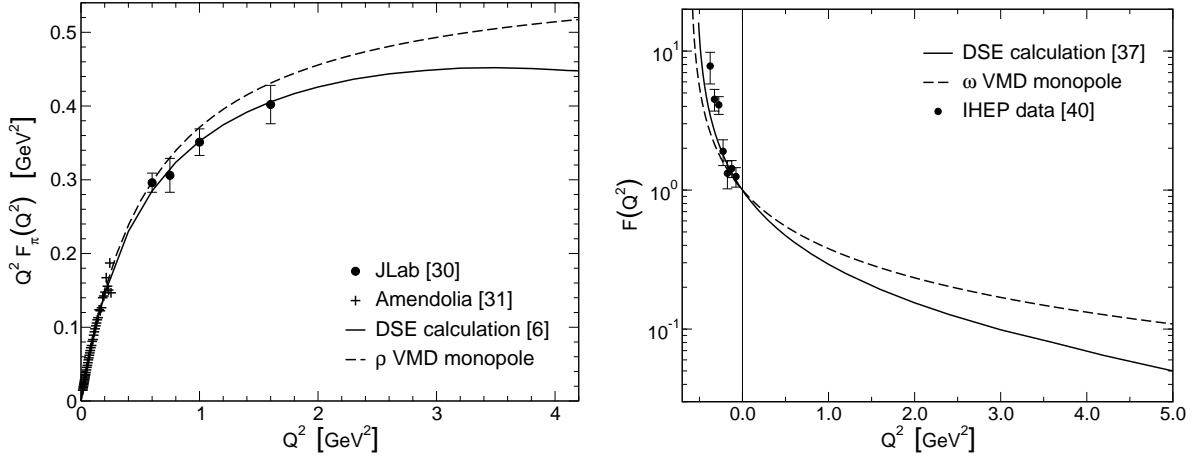


**Figure 3.** Left: The pion form factor  $Q^2 F_\pi(Q^2)$ , compared to the experimental results from Refs. [30,31]. Right: The transition form factor  $F_{\omega\pi\gamma}(Q^2)$  together with experimental data [40].

With photon momentum  $Q$ , and incoming and outgoing meson momenta  $P \mp Q/2$ , we can define a form factor for each of these diagrams [6]

$$2 P_\nu F_{ab;\bar{b}}(Q^2) = I_\nu^{a\bar{b};\bar{b}}(P - Q/2, Q, -(P + Q/2)). \quad (12)$$

We work in the isospin symmetric limit, and thus  $F_\pi(Q^2) = F_{u\bar{u};u}(Q^2)$ . The  $K^+$  and  $K^0$  form factors are given by  $F_{K^+} = \frac{2}{3}F_{u\bar{s};u} + \frac{1}{3}F_{u\bar{s};\bar{s}}$  and  $F_{K^0} = -\frac{1}{3}F_{d\bar{s};d} + \frac{1}{3}F_{d\bar{s};\bar{s}}$ , respectively.

Our result for  $Q^2 F_\pi$  are shown in the left panel of Fig. 3. In the timelike region, and in the spacelike region up to about  $Q^2 = 2 \text{ GeV}^2$ ,  $F_\pi$  can be described very well by a monopole with our calculated  $\rho$ -mass,  $m_\rho = 742 \text{ MeV}$  (note that our calculated  $\rho$ -mass is slightly below the experimental value). Above this value, our curve starts to deviate more and more from this naive vector meson dominance (VMD) monopole. Our result is in excellent agreement with the most recent JLab data [30]; it would be very interesting to compare with future JLab data in the 3 to 5  $\text{GeV}^2$  range, where we expect to see a significant deviation from the naive monopole behavior. The pQCD prediction is significantly smaller than our results at 4  $\text{GeV}^2$ ; we anticipate that true perturbative behavior sets in somewhere between 10 and 20  $\text{GeV}^2$  [32].

Recent lattice simulation also indicate that in the region between 0 and 2  $\text{GeV}^2$  the pion form factor can be represented by a VMD-like monopole [33,34]. This VMD-like behavior of the pion form factor in the spacelike region appears to be valid almost independent of the pion mass, both in our calculations and in the lattice simulations, though a monopole fit results in a VMD-mass which is slightly less than the actual vector meson mass. Current lattice simulations are not accurate enough, nor do they extend to large enough values of  $Q^2$ , to detect a significant deviation from VMD-like behavior above 2  $\text{GeV}^2$ .

Also our results [6] for  $F_K$  agree quite well with the available experimental data, as do both the neutral and the charged kaon charge radius [35,36], see Table 2. It should be noted here that the  $K^0$  form factor is obtained by taking the difference of two numbers,  $F_{d\bar{s};d}(Q^2)$  and  $F_{d\bar{s};\bar{s}}(Q^2)$ , which are both close to one for  $Q^2$  near zero. It is therefore much more sensitive to details of the model: both kaon loops and a flavor dependence of the (effective) quark-quark interaction will have a significantly bigger effect on the  $K^0$  form factor than on the  $K^+$  form factor. This could explain why it does not agree as well with experiment as our other results. In this respect one should note that the absolute deviation between our calculated charge radius and the experimental charge radius is similar for the charged and neutral kaon.

#### 4.2. Radiative vector-meson decays

We can describe the radiative decay of the vector mesons using the same loop integral, Eq. (10), this time with one vector meson BSA, one pseudoscalar BSA, and one  $q\bar{q}\gamma$ -vertex [37]. The generic structure of a vector-pseudoscalar-photon vertex is

$$I_{\mu\nu}^{a\bar{b};a}(P, Q, -(P+Q)) = \epsilon_{\mu\nu\alpha\beta} P_\alpha Q_\beta f_{a\bar{b};a}(Q^2), \quad (13)$$

where  $P$  is the vector momentum and  $Q$  the photon momentum. The on-shell value gives us the coupling constant, and can be used to calculate the partial decay width of the vector mesons. For virtual photons, we can define a transition form factor  $F_{VP\gamma}(Q^2)$ , normalized to 1 at  $Q^2 = 0$ , which can be used in estimating meson-exchange contributions to hadronic processes [38, 39].

In the isospin limit, both the  $\rho^0 \pi^0 \gamma$  and  $\rho^\pm \pi^\pm \gamma$  vertices are given by

$$\frac{g_{\rho\pi\gamma}}{m_\rho} \epsilon_{\mu\nu\alpha\beta} P_\alpha Q_\beta F_{\rho\pi\gamma}(Q^2) = \frac{1}{3} I_{\mu\nu}^{u\bar{u};u}(P, Q, -(P+Q)). \quad (14)$$

The  $\omega \pi \gamma$  vertex is a factor of 3 larger, due to the difference in isospin factors; however, the form factor  $F_{VP\gamma}(Q^2)$  is the same for  $\rho \pi \gamma$  and  $\omega \pi \gamma$ . In contrast to the elastic form factors, this transition form factor falls off significantly faster than a VMD-like monopole, as can be seen in the right panel of Fig. 3. Only in the timelike region, near the vector meson pole, do we see a true VMD-like behavior.

As Eq. (14) shows, it is  $g_{VP\gamma}/m_V$  that is the natural outcome of our calculations. Therefore, it is this combination that we give in Table 2, together with the corresponding partial decay widths [37]. As anticipated, the partial decay width  $\omega \rightarrow \pi\gamma$  is indeed (approximately) nine times larger than the  $\omega \rightarrow \pi\gamma$  partial decay width. Note that part of the difference between the experimental and calculated decay width comes from the phase space factor because our calculated vector meson masses deviate up to 5% from the physical masses.

For the  $K^* K \gamma$  decays (and corresponding form factors) [41] the situation is more complicated owing to the interference of the diagrams with the photon coupled to the  $s$ -quark and to the  $u$ - or  $d$ -quark. In the SU(3) flavor limit, the charged  $K^* K \gamma$  vertex becomes equal to the  $\rho \pi \gamma$  vertex, whereas the neutral  $K^* K \gamma$  vertex is twice as large in magnitude

$$\left(\frac{g_{K^* K \gamma}}{m_{K^*}}\right)^+ F_{K^* K \gamma}^+(Q^2) = \frac{2}{3} f_{u\bar{s};u}(Q^2) - \frac{1}{3} f_{u\bar{s};\bar{s}}(Q^2), \quad (15)$$

$$\left(\frac{g_{K^* K \gamma}}{m_{K^*}}\right)^0 F_{K^* K \gamma}^0(Q^2) = -\frac{1}{3} f_{d\bar{s};d}(Q^2) - \frac{1}{3} f_{u\bar{s};\bar{s}}(Q^2). \quad (16)$$

In Table 2 we see indeed that the partial decay width of the neutral  $K^* \rightarrow K\gamma$  is larger than that of the charged  $K^* \rightarrow K\gamma$ , though not by a factor of four as it would in the SU(3) flavor

**Table 2.** Overview of our results for the pseudoscalar-meson charge radii squared, all in  $\text{fm}^2$ , with an estimated combined numerical error of less than  $0.01 \text{ fm}^2$ . Also included are our results for the vector meson radiative decays:  $\Gamma_{V \rightarrow P\gamma}$  in  $\text{keV}$  and  $g/m$  in  $\text{GeV}^{-1}$ .

	$r_\pi^2$	$r_{K^+}^2$	$r_{K^0}^2$	$\Gamma_{\rho^\pm}$	$g/m$	$\Gamma_\omega$	$g/m$	$\Gamma_{K^{*\pm}}$	$g/m$	$\Gamma_{K^{*0}}$	$g/m$
calc.	0.44	0.38	-0.085	53	0.69	479	2.07	90	0.99	130	1.19
expt.	0.44	0.34(5)	-0.052(26)	68	0.74	757	2.38	50	0.84	116	1.27

limit. Furthermore, we see that the deviation between our calculation and experiment is largest for the charged  $K^* \rightarrow K\gamma$  decay. Again, this can be understood since this decay is sensitive to the difference between the impulse diagrams, and therefore more sensitive to details of the model and its omissions.

## Acknowledgments

We would like to thank Craig Roberts and Peter Tandy for useful discussions. This work was supported by the Austrian Research Foundation *FWF*, *Erwin-Schrödinger-Stipendium* no. J2233-N08, the Department of Energy, Office of Nuclear Physics, contract no. W-31-109-ENG-38, and benefited from the ANL Computing Resource Center's facilities; part of the computations were performed on the National Science Foundation Terascale Computing System at the Pittsburgh Supercomputing Center.

## References

- [1] C. D. Roberts and A. G. Williams, *Prog. Part. Nucl. Phys.* **33**, 477 (1994); C. D. Roberts and S. M. Schmidt, *Prog. Part. Nucl. Phys.* **45S1**, 1 (2000); R. Alkofer and L. von Smekal, *Phys. Rept.* **353**, 281 (2001).
- [2] P. Maris and C. D. Roberts, *Int. J. Mod. Phys. E* **12**, 297 (2003).
- [3] P. Maris and C. D. Roberts, *Phys. Rev. C* **56**, 3369 (1997).
- [4] P. Maris, C. D. Roberts and P. C. Tandy, *Phys. Lett. B* **420**, 267 (1998).
- [5] C. D. Roberts, *Nucl. Phys. A* **605**, 475 (1996).
- [6] P. Maris and P. C. Tandy, *Phys. Rev. C* **62**, 055204 (2000); P. Maris and P. C. Tandy, *Phys. Rev. C* **61**, 045202 (2000).
- [7] H. D. Politzer, *Nucl. Phys. B* **117**, 397 (1976).
- [8] K. Higashijima, *Phys. Rev. D* **29**, 1228 (1984).
- [9] P. I. Fomin, V. P. Gusynin, V. A. Miransky and Y. A. Sitenko, *Riv. Nuovo Cim.* **6N5**, 1 (1983).
- [10] J. I. Skullerud and A. G. Williams, *Phys. Rev. D* **63**, 054508 (2001); J. Skullerud, D. B. Leinweber and A. G. Williams, *Phys. Rev. D* **64**, 074508 (2001).
- [11] P. O. Bowman, U. M. Heller and A. G. Williams, *Phys. Rev. D* **66**, 014505 (2002).
- [12] J. B. Zhang, P. O. Bowman, D. B. Leinweber, A. G. Williams and F. D. R. Bonnet *Phys. Rev. D* **70**, 034505 (2004).
- [13] P. Maris, A. Raya, C. D. Roberts and S. M. Schmidt, *Eur. Phys. J. A* **18**, 231 (2003).
- [14] M. S. Bhagwat, M. A. Pichowsky, C. D. Roberts and P. C. Tandy, *Phys. Rev. C* **68**, 015203 (2003).
- [15] J. Skullerud and A. Kizilersu, *JHEP* **0209**, 013 (2002); J. I. Skullerud, P. O. Bowman, A. Kizilersu, D. B. Leinweber and A. G. Williams, *JHEP* **0304**, 047 (2003).
- [16] M. S. Bhagwat, A. Holl, A. Krassnigg, C. D. Roberts and P. C. Tandy, *Phys. Rev. C* **70**, 035205 (2004).
- [17] M. S. Bhagwat and P. C. Tandy, arXiv:hep-ph/0407163.
- [18] C. S. Fischer, F. J. Llanes-Estrada and R. Alkofer, arXiv:hep-ph/0407294; F. J. Llanes-Estrada, C. S. Fischer and R. Alkofer, arXiv:hep-ph/0407332.
- [19] C. S. Fischer and R. Alkofer, *Phys. Rev. D* **67**, 094020 (2003).
- [20] A. Bender, C. D. Roberts and L. Von Smekal, *Phys. Lett. B* **380**, 7 (1996).
- [21] A. Bender, W. Detmold, C. D. Roberts and A. W. Thomas, *Phys. Rev. C* **65**, 065203 (2002).
- [22] A. Krassnigg, W. Schweiger and W. H. Klink, *Phys. Rev. C* **67**, 064003 (2003).
- [23] A. Krassnigg and C. D. Roberts, arXiv:nucl-th/0308039.
- [24] A. Holl, A. Krassnigg and C. D. Roberts, *Phys. Rev. C* **70**, 042203 (2004).
- [25] M. A. Ivanov, Y. L. Kalinovsky and C. D. Roberts, *Phys. Rev. D* **60**, 034018 (1999).
- [26] P. Maris and P. C. Tandy, *Phys. Rev. C* **60**, 055214 (1999).
- [27] A. Hoell, A. Krassnigg, C. D. Roberts and S. V. Wright, arXiv:nucl-th/0411065.
- [28] S. Eidelman *et al.* [Particle Data Group Collaboration], *Phys. Lett. B* **592**, 1 (2004).
- [29] K. W. Edwards *et al.* [CLEO Collaboration], *Phys. Rev. Lett.* **86**, 30 (2001).
- [30] J. Volmer *et al.* [The Jefferson Lab F( $\pi$ ) Collaboration], *Phys. Rev. Lett.* **86**, 1713 (2001).
- [31] S. R. Amendolia *et al.* [NA7 Collaboration], *Nucl. Phys. B* **277**, 168 (1986).
- [32] P. Maris and C. D. Roberts, *Phys. Rev. C* **58**, 3659 (1998).
- [33] J. van der Heide, J. H. Koch and E. Laermann, *Phys. Rev. D* **69**, 094511 (2004).
- [34] F. D. R. Bonnet, R. G. Edwards, G. T. Fleming, R. Lewis and D. G. Richards arXiv:hep-lat/0411028.
- [35] S. R. Amendolia *et al.*, *Phys. Lett. B* **178**, 435 (1986).
- [36] W. R. Molzon *et al.*, *Phys. Rev. Lett.* **41**, 1213 (1978) [Erratum-ibid. **41**, 1523 (1978 ERRAT,41,1835.1978)].



- [37] P. Maris and P. C. Tandy, *Phys. Rev. C* **65**, 045211 (2002).
- [38] J. W. Van Orden, N. Devine and F. Gross, *Phys. Rev. Lett.* **75**, 4369 (1995).
- [39] P. C. Tandy, *Prog. Part. Nucl. Phys.* **39**, 117 (1997).
- [40] R. I. Dzhelezhyan *et al.*, *Phys. Lett. B* **102**, 296 (1981) [*JETP Lett.* **33**, 228 (1981)].
- [41] P. Maris, arXiv:nucl-th/0209048.